ACS Photonics

Article

pubs.acs.org/journal/apchd5

Active Control of Graphene-Based Unidirectional Surface Plasmon Launcher

Yanjun Bao,[†] Shuai Zu,[†] Yifei Zhang,[†] and Zheyu Fang*[,†,‡]

[†]School of Physics, State Key Lab for Mesoscopic Physics, Peking University, Beijing 100871, China

[‡]Collaborative Innovation Center of Quantum Matter, Beijing 100871, China

Supporting Information

ABSTRACT: The manipulation of surface plasmon polariton (SPP) propagation is a basic subject for the realization of novel optical devices. Although the unidirectional SPP launcher has been demonstrated, it has been difficult to realize active control suitable for device applications. Here, we propose a graphene device with electrically controllable propagation of SPPs. The source/drain electrode of this device is made of a reflective antenna pair structure, with its optical resonance controlled by the corresponding applied voltage. With appropriate source and drain bias, this device can serve as a good unidirectional SPP launcher, with a high extinction ratio over 2000 and generation efficiency of 0.38. The electrical control allows us to tune the propagation of SPPs with significant flexibility, which may be used for future novel plasmonic devices and photonic circuits.

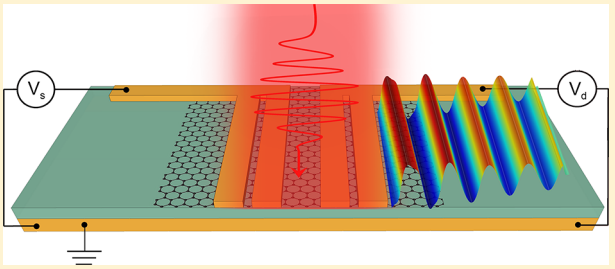

KEYWORDS: *surface plasmon polaritons (SPPs), unidirectional SPP launcher, graphene device, reflective antenna pair (RAP), effective circuit model*

Plasmonics, which is concerned with the coupling between light and surface plasmon polaritons (SPPs), has become a research hotspot in recent years.[1,2] Due to the unique properties of subwavelength confinement and significant field enhancement of SPPs, it has been used in many optical devices including modulators,[3,4] waveguides,[5−7] and switches.[8] One of the fundamental issues in plasmonics is to manipulate the propagation direction of SPPs. Many approaches have been proposed to generate a unidirectional launching of SPPs to realize optical devices, which can be classified into two types: passive and active control. The passive device refers to that in which SPPs propagate without any additional external control, such as a slit near the Bragg grating,[9] dislocated double-layer gratings,[10] two compact nanoantennas,[11] and asymmetric grooves.[12] An active device, on the other hand, involving an external input that controls the propagation behavior of SPPs, can extend the range of its applications even further. These external inputs include the polarization of light,[13,14] the position of the dipole source,[15] the illumination angle,[16,17] etc.

Graphene, a single layer of carbon atoms arranged in a honeycomb lattice, exhibits superior electronic and mechanical properties[18−20] and has been recognized as a suitable material for photonic and optoelectronic applications.[21−29] More importantly, the conductivity of graphene can be continuously tuned from infrared to THz frequencies by electrostatic doping,[30−32] which enables fast switch and on-chip integration. When graphene is introduced into metallic structures, controllable plasmonic resonances can be obtained,[33−37] demonstrating graphene as a promising candidate for active tuning of plasmonic structures. Inspired by this, we think it is possible that the SPP propagation in graphene-incorporated plasmonic structures can be actively controlled by external electrostatic voltages.

In this article, we first propose a graphene-loaded reflective antenna pair (RAP) structure and investigate its resonance wavelength dependence on the Fermi level of graphene. Then we develop a circuit model to understand the large tuning effect induced by the graphene. On the basis of this structure, we propose a graphene device in which the RAP structures are used as the source and drain electrodes. We find that this device can serve as a good unidirectional SPP launcher with appropriate source and drain voltages. Finally, the extinction ratios of the device with different source and drain voltages are investigated.

GRAPHENE-LOADED RAP STRUCTURE AND ITS RESONANCE PROPERTIES

Figure 1a illustrates the geometry of the graphene-loaded RAP structure. A pair of nanostrips coupled with a graphene sheet are separated by a SiO_2 spacer from an Au mirror substrate, which prevents the light transmission. The Fermi level of graphene is controlled by a bias voltage applied between the antenna pair and the Au substrate. A plane wave of TM polarization (magnetic field H_z is perpendicular to the $x-y$ plane) impinges normally on the top of the structure. The refractive index of the SiO_2 spacer is taken as 1.4, and the

Received: April 10, 2015
Published: June 29, 2015

DOI: 10.1021/acsphotonics.5b00182
ACS Photonics 2015, 2, 1135−1140

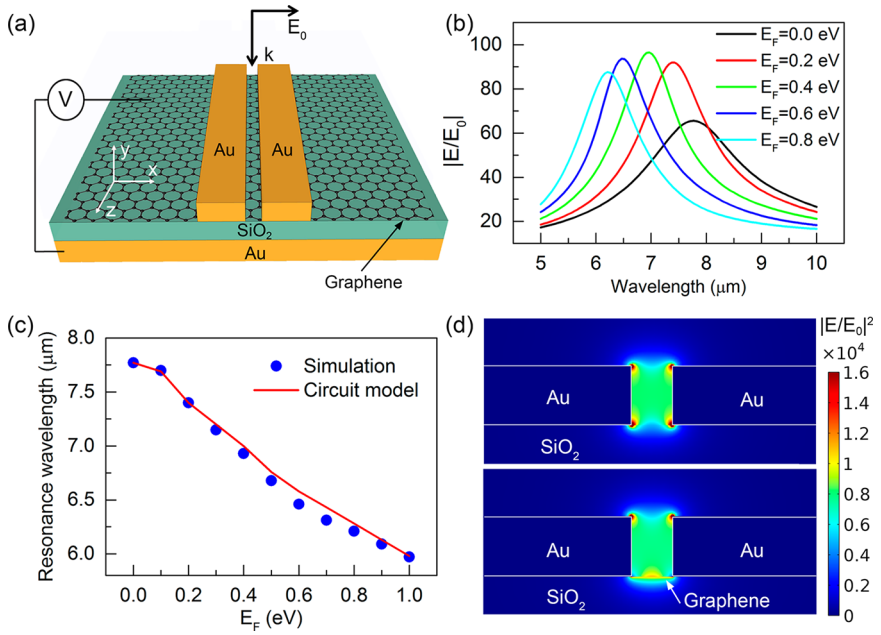

Figure 1. (a) Schematic view of the graphene-loaded RAP structure. The width and the thickness of each nanostrip are 1.7 μm and 50 nm, respectively. The gap between the two nanostrips is g = 30 nm. The thickness of the SiO_2 spacer is 150 nm, and the thickness of the Au mirror is 200 nm. (b) Magnitude of the electric field $|E/E_0|$ at the center of the gap with difference Fermi level of the graphene. (c) Resonance wavelength of the RAP structure as a function of the Fermi level of the graphene E_F obtained from the simulation (blue solid circles) and circuit model (red line). (d) Electric field intensity distributions in the vicinity of the gap at the z = 0 nm plane without (upper panel) and with (lower panel) the graphene sheet. The white lines denote the boundaries of the Au regions.

permittivity of gold is obtained by fitting the experimental data from the literature.[38] The surface conductivity of graphene used in our calculation is derived with the random-phase approximation,[39] including the effect of finite temperature (T = 300 K):

$$\sigma_s(\omega) = \frac{2ie^2k_BT}{\pi\hbar^2(\omega + i\tau^{-1})}\ln\left[2\cosh\left(\frac{E_F}{2k_BT}\right)\right] + \frac{e^2}{4\pi\hbar}\left\{-\frac{i}{2}\ln\frac{(\hbar\omega + 2E_F)^2}{(\hbar\omega - 2E_F)^2 + (2k_BT)^2} + \frac{\pi}{2} + \arctan\left(\frac{\hbar\omega - 2E_F}{2k_BT}\right)\right\} \quad (1)$$

where $-e$ is the charge of an electron, $\hbar = h/2\pi$ is the reduced Planck's constant, k_B is the Boltzmann's constant, ω is the radian frequency, and E_F is the Fermi energy of the graphene. The carrier scattering time τ used in the model is estimated from the mobility of graphene (μ = 3000 $cm^2/V{\cdot}s$) through the expression $\tau = \mu E_F/ev_F^2$, where $v_F = 10^6$ m/s is the Fermi velocity of graphene. The in-plane permittivity of the graphene can be obtained as

$$\varepsilon_{\parallel} = 1 + \frac{i\sigma}{\omega\varepsilon_0} = 1 + \frac{i\sigma_s}{\omega\varepsilon_0 t_G} \quad (2)$$

where t_G is the thickness of the graphene and is assumed to be 0.33 nm in the calculation. With the increase of the Fermi level of graphene, the real part of the permittivity decreases (see Figure S1), which can be used to tune the resonance of the antennas. The out-of-plane permittivity of graphene is kept as 2.25.

Figure 1b shows the magnitude of the electric field at the center of the gap with different Fermi levels of the graphene. One can clearly see that a resonance peak is observed for each curve. The simulated resonance wavelength dependence on the Fermi level of the graphene is shown in Figure 1c (blue solid circles). When the graphene Fermi level increases from 0.0 to 1.0 eV, the resonance blue shifts 1.75 μm. To understand the large tuning effect, we plot the electric field intensity distributions in the vicinity of the gap with and without the graphene. For both situations, due to the reflective metallic mirror, the electric field is strongly enhanced and localized between the gaps (Figure 1d). Nevertheless, for the case with graphene (lower panel), the electric field concentrates its energy near the graphene region, which contributes to the large tuning of the antenna resonance. Because the intensity of the electric field is highly localized within the gap, the effect of graphene outside the antenna gap is almost negligible.[34]

EFFECTIVE CIRCUIT MODEL OF THE GRAPHENE-LOADED RAP STRUCTURE

To obtain insight into the tuning effect, we establish a circuit model for the antenna resonance. Figure 2a shows the effective circuit model for the RAP structure without the graphene. In this model, the Au metals can be interpreted as resistance and inductance, and the dielectric materials (such as the antenna gap and the SiO_2 spacer) can be represented as capacitance. The input impedance Z_R, defined as the ratio of the voltage across the gap to the total induced displacement current, can be calculated as

$$\frac{1}{Z_R} = -i\omega C_1 + \frac{1}{R - i\omega L - 2/i\omega C_2} \quad (3)$$

The obtained impedance of Z_R based on this effective circuit model is plotted in Figure 2c (blue lines). It agrees well with the full wave simulation result (red lines), which is obtained by placing a discrete current source at the empty antenna gap.

DOI: 10.1021/acsphotonics.5b00182
ACS Photonics 2015, 2, 1135−1140

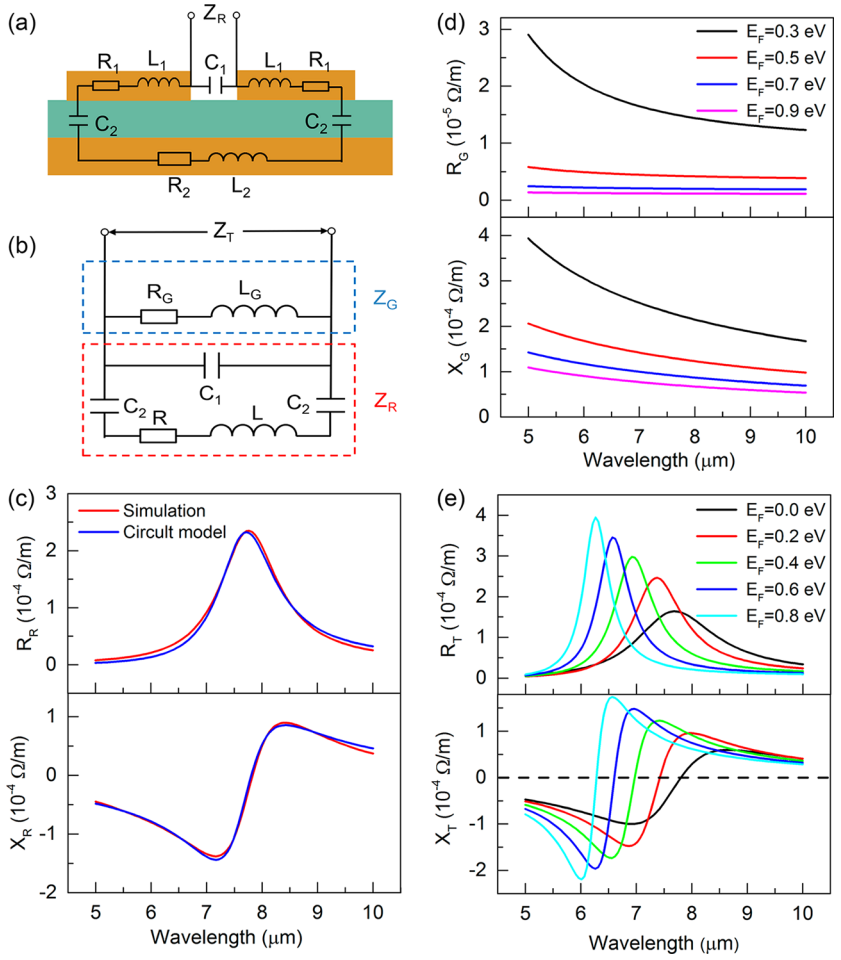

Figure 2. (a, b) Circuit model of the RAP structure without (a) and with (b) graphene. The impedances of the RAP, the loaded graphene, and the graphene-loaded RAP structure are denoted as Z_R, Z_G, and Z_T, respectively. In (b), $R = 2R_1 + R_2$, $L = 2L_1 + L_2$. All symbols are defined per unit length. (c) RAP impedance $Z_R = (R_R - iX_R)$ obtained with the effective circuit model ($C_1 = 8.56 \times 10^{-11}$ F/m, $C_2 = 6.08 \times 10^{-10}$ F/m, $L = 2.48 \times 10^{-19}$ H/m, $R = 9.8 \times 10^{-6}$ Ω/m) and full wave simulation. (d) Resistance (R_G) and reactance (X_G) of the graphene loaded in the gap ($g = 30$ nm, $t_G = 0.33$ nm). (e) Resistance (R_T) and reactance (X_T) of the graphene-loaded RAP structure for different Fermi levels of the graphene. The black dashed line corresponds to the zero value of the reactance.

When the graphene is loaded at the gap, the incident electric field drives the electrons in the graphene to flow along the x direction. The voltage across the graphene is $V = gE_x$ and the current (times unit length along the z axis) is $I = Jt_G$. Then the graphene impedance at the gap can be calculated as[34]

$$Z_G = \frac{V}{I} = \frac{gE_x}{Jt_G} = \frac{g}{(\sigma - i\omega\varepsilon_0)t_G} = \frac{g}{-i\omega\varepsilon_0\varepsilon_{//}t_G} \quad (4)$$

The calculated graphene impedance is shown in Figure 2d. As the Fermi level increases, both the resistance (R_G) and reactance (X_G) decrease. Because the real part of the graphene permittivity is negative in the considered wavelength range, the reactance (X_G) of the graphene can be positive, which indicates that the graphene load can be interpreted as a positive inductance L_G ($=X_G/\omega$), as shown in Figure 2b.

With the impedance of the graphene Z_G parallel to the RAP impedance Z_R (Figure 2b), the total impedance Z_T can be directly calculated as $Z_T^{-1} = Z_R^{-1} + Z_G^{-1}$, which is shown in Figure 2e. As the Fermi level of the graphene increases, the peak wavelength of the resistance decreases. The resonance wavelength, defined as where the reactance X_T is zero (dashed black line in Figure 2e), is extracted and plotted in Figure 1c (red line), which agrees well with the simulation results. The good agreement demonstrates that the effective circuit model is a powerful tool for the study of the resonance behavior of the antenna structures.

UNIDIRECTIONAL LAUNCHING OF SPPS IN A GRAPHENE DEVICE

Based on the RAP structure, we propose a graphene device in which the unidirectional excitation of SPPs can be actively controlled, as shown in Figure 3a. The device consists of two pairs of antenna structures that serve as the source and drain electrodes, where the geometric parameters are the same as in Figure 1a. Underneath the electrodes, a layer of graphene is placed on the top of the dielectric spacer. Source and drain voltages are applied between the paired antenna structures and the Au substrate, with the back gate taken as the ground. This design enables the Fermi level of graphene loaded at the electrode gaps to be directly controlled by the source and drain voltages, while that of the graphene between the two electrodes shows a spatially variant value along the x direction.[40] Here, we are not interested in the graphene located outside the electrode gaps, because they have little effect on the resonance of the RAP structure. A plane TM wave at a wavelength of 6.4 μm normally illuminates the whole structure, with a center-to-

DOI: 10.1021/acsphotonics.5b00182
ACS Photonics 2015, 2, 1135−1140

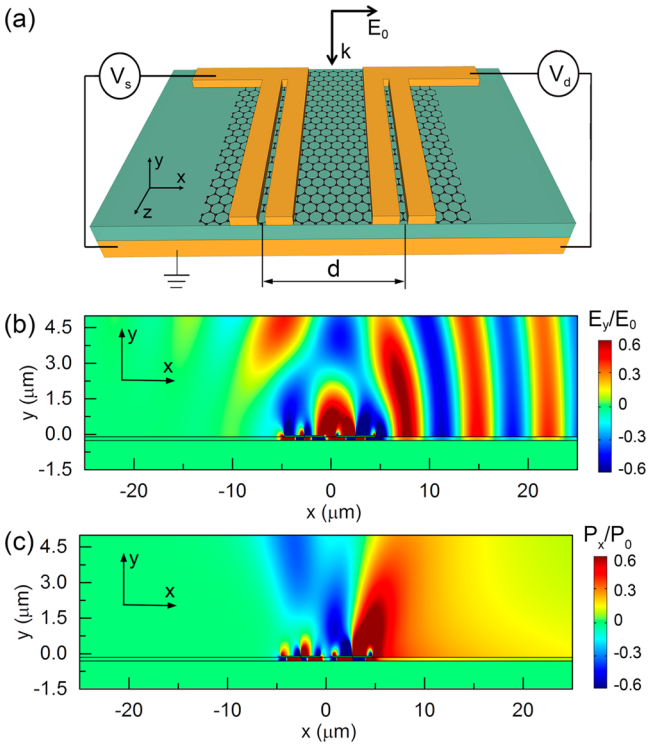

Figure 3. (a) Schematic of the graphene device with active control of SPPs. RAP structures serve as the source and drain electrodes with a center to center distance of d = 4.8 μm. The y component of the electric field distribution (b) and the x component of the Poynting vector distribution (c) at the x–y plane for 6.4 μm incident wavelength when the Fermi level of the graphene loaded at the source and drain electrodes are 0.2 and 0.8 eV, respectively.

center distance between the two electrodes of d = 4.8 μm, which is about three-quarters of the incident wavelength. Figure 3b shows a cross sectional view of the electric field distribution at the x–y plane when the Fermi level of the graphene loaded at the gaps of the source and drain electrodes is 0.2 and 0.8 eV, respectively. One can see that the SPPs mainly propagate to the right side along the surface of the gold substrate, with an SPP wavelength close to the incident wavelength. Thus, the observed SPPs are not graphene plasmons, which have a typical wavelength of several hundreds of nanometers and decay within a few plasmon wavelengths.[41] To show the unidirectional propagation more clearly, we also plot the power flow of Poynting vectors in Figure 3c, where the unidirectional launching of SPPs to the right side can be clearly observed. Due to the large real and imaginary parts of the permittivity of gold in the mid-infrared frequencies, the SPPs are highly delocalized and extend over a great number of wavelengths into the air space above the interface (Figure 3b), which is also known as Sommerfeld–Zenneck waves.[42] When the gold substrate is periodically corrugated, the SPPs can be strongly bound along the interface, while still maintaining a good unidirectional propagation property (see Figure S2).

To quantify the directionality of the device, we first introduce the SPP generation efficiency to one side η, which is defined as the SPP power flowing in a certain propagation direction normalized by the light power incident on the two electrodes. The extinction ratio, as a measure of the unidirectional performance of the device, is defined as $E_R = \eta_R/\eta_L$, where η_R and η_L represent the SPP generation efficiencies to the right and left, respectively. For the device, the total SPP generation efficiency ($\eta_T = \eta_R + \eta_L$) is 0.38, and the extinction ratio is about 2500. The high extinction ratio and generation efficiency show that our device is an efficient unidirectional SPP launcher in comparison with others.[9,10]

The gold mirror in our device is used to support the propagation of SPPs and also enhances the phase tuning of the antenna structure.[33] Figure 4a shows the resonance phases of the RAP structure with Fermi levels of 0.2 and 0.8 eV. The relative phase difference between the two resonators is shown as the black line. At an incident wavelength of 6.4 μm, a phase difference of $\sim\pi/2$ is obtained (green dashed line in Figure 4a), which can be used for understanding the unidirectional launching of SPPs in the device. As known, a nanostrip and a metallic mirror separated by a dielectric spacer can be represented as a magnetic resonator,[43] which can be modeled as a magnetic dipole oscillating along the z axis, due to its subwavelength dimensions. For our device, the structure is modeled as four magnetic dipoles (Figure 4b), where the left (right) two magnetic dipoles have the same phases as that of

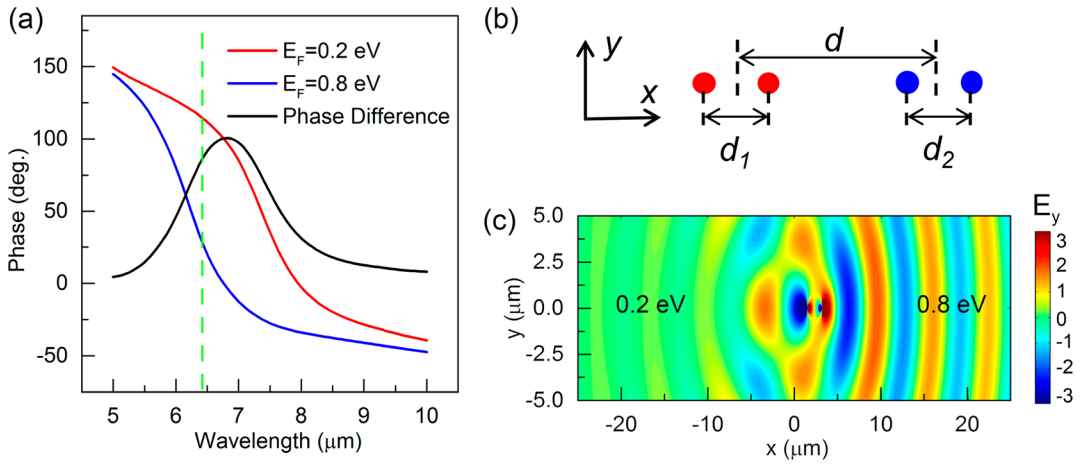

Figure 4. (a) Phases of the resonance for the RAP structure with a Fermi level of 0.2 and 0.8 eV, respectively. The black line shows the phase difference between the two cases. The dashed green line corresponds to the wavelength of 6.4 μm. (b) Schematic of the magnetic dipole (solid circles) approximation. The orientation of the four magnetic dipoles is along the z axis. The distances between the dipoles are $d_1 = d_2$ = 1.7 μm and d = 4.8 μm. (c) The y component of the electric field distributions excited by the four magnetic dipoles.

DOI: 10.1021/acsphotonics.5b00182
ACS Photonics 2015, 2, 1135–1140

the RAP structure with a Fermi level of 0.2 eV (0.8 eV). With an appropriate distance between the four magnetic dipoles, the emissions interfere constructively in one direction and destructively in the opposite direction, resulting in directional propagation of electromagnetic (EM) waves. In order to confirm this prediction, we simulate the field distribution excited by four magnetic dipoles at a wavelength of 6.4 μm in the $x-y$ plane, as shown in Figure 4c. As expected, the EM waves primarily propagate to the right, and the one along the opposite direction is strongly suppressed. With such a simple model, we can explain the main features of this unidirectional SPP propagation without considering other factors, such as the quadrupolar mode and phase retardation of the magnetic resonator.

Finally, we show how the unidirectional propagation of the SPPs can be electrically controlled. Figure 5 shows a mapping

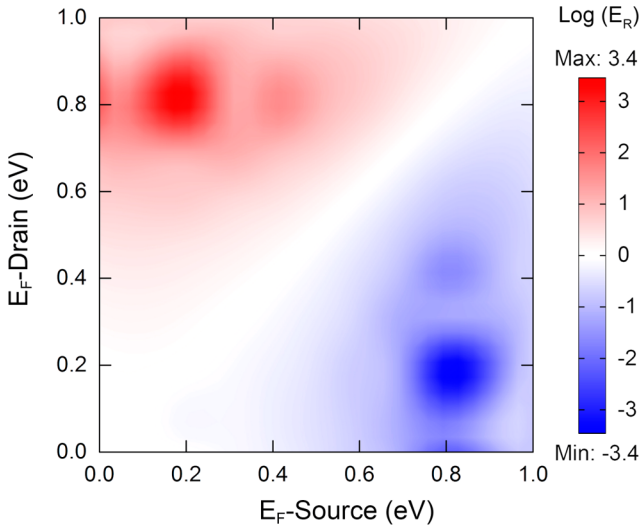

Figure 5. Extinction ratio dependence on the Fermi level of the graphene loaded at the gaps of the source and drain electrodes.

of the extinction ratio dependence on the Fermi level of the graphene loaded at the gaps of the source and drain electrodes. It is clearly seen that the propagation of SPPs is strongly dependent on the source and drain voltages. The highest extinction ratio of $10^{3.4}$ is achieved when the Fermi level of graphene loaded at the source and drain electrodes is 0.2 and 0.8 eV, respectively. When the source and drain voltages are reversed, the extinction ratio reaches a minimum at about $10^{-3.4}$, meaning that the SPPs mainly propagate along the left side.

In conclusion, we have proposed a graphene device in which the unidirectional SPP propagation can be actively tuned by the source and drain voltages. The key part of the device is the design of the electrodes, in which the optical resonance can be controlled by the applied voltage. The SPPs generated by the source and drain electrodes interfere constructively or destructively in one direction, resulting in directional SPP propagation. Moreover, compared with other unidirectional SPP launchers,[9,10] the device in this study provides simultaneously high generation efficiency (~0.38) and a high extinction ratio (>2000). We believe that our graphene device, with significant flexibility for controlling the propagation of SPPs, may form the basis for novel plasmonic devices and active plasmonic photonic circuits in the future.

■ ASSOCIATED CONTENT

Supporting Information

The Supporting Information includes (1) the graphene permittivity calculated with RPA at T = 300 K for different Fermi levels of single-layer graphene and (2) the electric field distribution at the $x-y$ plane when the gold substrate is periodically corrugated. The Supporting Information is available free of charge on the ACS Publications website at DOI: 10.1021/acsphotonics.5b00182.

■ AUTHOR INFORMATION

Corresponding Author

*E-mail: zhyfang@pku.edu.cn.

Notes

The authors declare no competing financial interest.

■ ACKNOWLEDGMENTS

This work is supported by National Science Foundation of China (Grant Nos. 61422501 and 11374023), the National Basic Research Program of China (973 Program, Grant No. 2015CB932403), Beijing Natural Science Foundation (Grant No. L140007), and Foundation for the Author of National Excellent Doctoral Dissertation of PR China (Grant No. 201420).

■ REFERENCES

(1) Ozbay, E. Plasmonics: merging photonics and electronics at nanoscale dimensions. *Science* **2006**, *311*, 189−193.
(2) Gramotnev, D. K.; Bozhevolnyi, S. I. Plasmonics beyond the diffraction limit. *Nat. Photonics* **2010**, *4*, 83−91.
(3) Cai, W. S.; White, J. S.; Brongersma, M. L. Compact, High-Speed and Power-Efficient Electrooptic Plasmonic Modulators. *Nano Lett.* **2009**, *9*, 4403−4411.
(4) Melikyan, A.; Alloatti, L.; Muslija, A.; Hillerkuss, D.; Schindler, P. C.; Li, J.; Palmer, R.; Korn, D.; Muehlbrandt, S.; Van Thourhout, D.; Chen, B.; Dinu, R.; Sommer, M.; Koos, C.; Kohl, M.; Freude, W.; Leuthold, J. High-speed plasmonic phase modulators. *Nat. Photonics* **2014**, *8*, 229−233.
(5) Pyayt, A. L.; Wiley, B.; Xia, Y.; Chen, A.; Dalton, L. Integration of photonic and silver nanowire plasmonic waveguides. *Nat. Nanotechnol.* **2008**, *3*, 660−665.
(6) Christensen, J.; Manjavacas, A.; Thongrattanasiri, S.; Koppens, F. H. L.; de Abajo, F. J. G. Graphene Plasmon Waveguiding and Hybridization in Individual and Paired Nanoribbons. *ACS Nano* **2012**, *6*, 431−440.
(7) Li, Z.; Kou, J. L.; Kim, M.; Lee, J. O.; Choo, H. Highly Efficient and Tailorable On-Chip Metal-Insulator-Metal Plasmonic Nano-focusing Cavity. *ACS Photonics* **2014**, *1*, 944−953.
(8) Chang, W. S.; Lassiter, J. B.; Swanglap, P.; Sobhani, H.; Khatua, S.; Nordlander, P.; Halas, N. J.; Link, S. A plasmonic Fano switch. *Nano Lett.* **2012**, *12*, 4977−4982.
(9) López-Tejeira, F.; Rodrigo, S. G.; Martín-Moreno, L.; García-Vidal, F. J.; Devaux, E.; Ebbesen, T. W.; Krenn, J. R.; Radko, I. P.; Bozhevolnyi, S. I.; González, M. U.; Weeber, J. C.; Dereux, A. Efficient unidirectional nanoslit couplers for surface plasmons. *Nat. Phys.* **2007**, *3*, 324−328.
(10) Liu, T.; Shen, Y.; Shin, W.; Zhu, Q.; Fan, S.; Jin, C. Dislocated double-layer metal gratings: an efficient unidirectional coupler. *Nano Lett.* **2014**, *14*, 3848−3854.
(11) Liu, Y.; Palomba, S.; Park, Y.; Zentgraf, T.; Yin, X.; Zhang, X. Compact magnetic antennas for directional excitation of surface plasmons. *Nano Lett.* **2012**, *12*, 4853−4858.
(12) Huang, X.; Brongersma, M. L. Compact aperiodic metallic groove arrays for unidirectional launching of surface plasmons. *Nano Lett.* **2013**, *13*, 5420−5424.

DOI: 10.1021/acsphotonics.5b00182
ACS Photonics 2015, 2, 1135−1140

(13) Lin, J.; Mueller, J. P.; Wang, Q.; Yuan, G.; Antoniou, N.; Yuan, X. C.; Capasso, F. Polarization-controlled tunable directional coupling of surface plasmon polaritons. *Science* **2013**, *340*, 331−334.
(14) Rodriguez-Fortuno, F. J.; Marino, G.; Ginzburg, P.; O'Connor, D.; Martinez, A.; Wurtz, G. A.; Zayats, A. V. Near-field interference for the unidirectional excitation of electromagnetic guided modes. *Science* **2013**, *340*, 328−330.
(15) Dong, Z.; Chu, H.-S.; Zhu, D.; Du, W.; Akimov, Y. A.; Goh, W. P.; Wang, T.; Goh, K. E. J.; Troadec, C.; Nijhuis, C. A.; Yang, J. K. W. Electrically-Excited Surface Plasmon Polaritons with Directionality Control. *ACS Photonics* **2015**, *2*, 385−391.
(16) Kim, H.; Lee, B. Unidirectional Surface Plasmon Polariton Excitation on Single Slit with Oblique Backside Illumination. *Plasmonics* **2009**, *4*, 153−159.
(17) Radko, I. P.; Bozhevolnyi, S. I.; Brucoli, G.; Martin-Moreno, L.; Garcia-Vidal, F. J.; Boltasseva, A. Efficient unidirectional ridge excitation of surface plasmons. *Opt. Express* **2009**, *17*, 7228−7232.
(18) Novoselov, K. S.; Geim, A. K.; Morozov, S. V.; Jiang, D.; Katsnelson, M. I.; Grigorieva, I. V.; Dubonos, S. V.; Firsov, A. A. Two-dimensional gas of massless Dirac fermions in graphene. *Nature* **2005**, *438*, 197−200.
(19) Novoselov, K. S.; Geim, A. K.; Morozov, S. V.; Jiang, D.; Zhang, Y.; Dubonos, S. V.; Grigorieva, I. V.; Firsov, A. A. Electric field effect in atomically thin carbon films. *Science* **2004**, *306*, 666−669.
(20) Chen, C. Y.; Lee, S.; Deshpande, V. V.; Lee, G. H.; Lekas, M.; Shepard, K.; Hone, J. Graphene mechanical oscillators with tunable frequency. *Nat. Nanotechnol.* **2013**, *8*, 923−927.
(21) Bonaccorso, F.; Sun, Z.; Hasan, T.; Ferrari, A. C. Graphene photonics and optoelectronics. *Nat. Photonics* **2010**, *4*, 611−622.
(22) Fang, Z.; Liu, Z.; Wang, Y.; Ajayan, P. M.; Nordlander, P.; Halas, N. J. Graphene-antenna sandwich photodetector. *Nano Lett.* **2012**, *12*, 3808−3813.
(23) Fang, Z. Y.; Thongrattanasiri, S.; Schlather, A.; Liu, Z.; Ma, L. L.; Wang, Y. M.; Ajayan, P. M.; Nordlander, P.; Halas, N. J.; de Abajo, F. J. G. Gated Tunability and Hybridization of Localized Plasmons in Nanostructured Graphene. *ACS Nano* **2013**, *7*, 2388−2395.
(24) Fang, Z. Y.; Wang, Y. M.; Liu, Z.; Schlather, A.; Ajayan, P. M.; Koppens, F. H. L.; Nordlander, P.; Halas, N. J. Plasmon-Induced Doping of Graphene. *ACS Nano* **2012**, *6*, 10222−10228.
(25) Manjavacas, A.; Nordlander, P.; de Abajo, F. J. G. Plasmon Blockade in Nanostructured Graphene. *ACS Nano* **2012**, *6*, 1724−1731.
(26) Zhu, X. L.; Shi, L.; Schmidt, M. S.; Boisen, A.; Hansen, O.; Zi, J.; Xiao, S. S.; Mortensen, N. A. Enhanced Light-Matter Interactions in Graphene-Covered Gold Nanovoid Arrays. *Nano Lett.* **2013**, *13*, 4690−4696.
(27) Zhu, X. L.; Yan, W.; Mortensen, N. A.; Xiao, S. S. Bends and splitters in graphene nanoribbon waveguides. *Opt. Express* **2013**, *21*, 3486−3491.
(28) Lamata, I. S.; Alonso-Gonzalez, P.; Hillenbrand, R.; Nikitin, A. Y. Plasmons in Cylindrical 2D Materials as a Platform for Nanophotonic Circuits. *ACS Photonics* **2015**, *2*, 280−286.
(29) Garcia de Abajo, F. J. G. Graphene Plasmonics: Challenges and Opportunities. *ACS Photonics* **2014**, *1*, 135−152.
(30) Hanson, G. W. Dyadic Green's functions and guided surface waves for a surface conductivity model of graphene. *J. Appl. Phys.* **2008**, *103*, 064302.
(31) Koppens, F. H.; Chang, D. E.; Garcia de Abajo, F. J. Graphene plasmonics: a platform for strong light-matter interactions. *Nano Lett.* **2011**, *11*, 3370−3377.
(32) Fang, Z.; Wang, Y.; Schlather, A. E.; Liu, Z.; Ajayan, P. M.; de Abajo, F. J.; Nordlander, P.; Zhu, X.; Halas, N. J. Active tunable absorption enhancement with graphene nanodisk arrays. *Nano Lett.* **2014**, *14*, 299−304.
(33) Li, Z.; Yu, N. Modulation of mid-infrared light using graphene-metal plasmonic antennas. *Appl. Phys. Lett.* **2013**, *102*, 131108.
(34) Yao, Y.; Kats, M. A.; Genevet, P.; Yu, N.; Song, Y.; Kong, J.; Capasso, F. Broad electrical tuning of graphene-loaded plasmonic antennas. *Nano Lett.* **2013**, *13*, 1257−1264.
(35) Zhu, X.; Shi, L.; Schmidt, M. S.; Boisen, A.; Hansen, O.; Zi, J.; Xiao, S.; Mortensen, N. A. Enhanced light-matter interactions in graphene-covered gold nanovoid arrays. *Nano Lett.* **2013**, *13*, 4690−4696.
(36) Emani, N. K.; Chung, T. F.; Ni, X. J.; Kildishev, A. V.; Chen, Y. P.; Boltasseva, A. Electrically Tunable Damping of Plasmonic Resonances with Graphene. *Nano Lett.* **2012**, *12*, 5202−5206.
(37) Dabidian, N.; Kholmanov, I.; Khanikaev, A. B.; Tatar, K.; Trendafilov, S.; Mousavi, S. H.; Magnuson, C.; Ruoff, R. S.; Shvets, G. Electrical Switching of Infrared Light Using Graphene Integration with Plasmonic Fano Resonant Metasurfaces. *ACS Photonics* **2015**, *2*, 216−227.
(38) Johnson, P. B.; Christy, R. W. Optical Constants of the Noble Metals. *Phys. Rev. B* **1972**, *6*, 4370−4379.
(39) Falkovsky, L. A.; Pershoguba, S. S. Optical far-infrared properties of a graphene monolayer and multilayer. *Phys. Rev. B: Condens. Matter Mater. Phys.* **2007**, *76*, 153410.
(40) Chen, P. Y.; Huang, H. Y.; Akinwande, D.; Alu, A. Graphene-Based Plasmonic Platform for Reconfigurable Terahertz Nanodevices. *ACS Photonics* **2014**, *1*, 647−654.
(41) Fei, Z.; Rodin, A. S.; Andreev, G. O.; Bao, W.; McLeod, A. S.; Wagner, M.; Zhang, L. M.; Zhao, Z.; Thiemens, M.; Dominguez, G.; Fogler, M. M.; Castro Neto, A. H.; Lau, C. N.; Keilmann, F.; Basov, D. N. Gate-tuning of graphene plasmons revealed by infrared nano-imaging. *Nature* **2012**, *487*, 82−85.
(42) Goubau, G. Surface Waves and Their Application to Transmission Lines. *J. Appl. Phys.* **1950**, *21*, 1119−1128.
(43) Shalaev, V. M. Optical negative-index metamaterials. *Nat. Photonics* **2007**, *1*, 41−48.

DOI: 10.1021/acsphotonics.5b00182
ACS Photonics 2015, 2, 1135−1140